Hindawi Publishing Corporation
Journal of Nanotechnology
Volume 2014, Article ID 102404, 19 pages
http://dx.doi.org/10.1155/2014/102404

Hindawi

Review Article

Silicon Nanofabrication by Atomic Force Microscopy-Based Mechanical Processing

Shojiro Miyake,[1] Mei Wang,[2] and Jongduk Kim[3]

[1] *Department of Innovative System Engineering, Nippon Institute of Technology, Miyashiro-machi, Saitama 345-8501, Japan*
[2] *R&D OSG Corporation, Honnogahara 1-15, Toyokawa 442-8544, Japan*
[3] *Park Systems Japan Inc., 1-17-1 Kanda-Nishikicho, Chiyoda-ku, Tokyo 101-0054, Japan*

Correspondence should be addressed to Mei Wang; wmei64@yahoo.com

Received 17 December 2013; Revised 3 April 2014; Accepted 7 April 2014; Published 11 May 2014

Academic Editor: Federico Rosei

Copyright © 2014 Shojiro Miyake et al. This is an open access article distributed under the Creative Commons Attribution License, which permits unrestricted use, distribution, and reproduction in any medium, provided the original work is properly cited.

This paper reviews silicon nanofabrication processes using atomic force microscopy (AFM). In particular, it summarizes recent results obtained in our research group regarding AFM-based silicon nanofabrication through mechanochemical local oxidation by diamond tip sliding, as well as mechanical, electrical, and electromechanical processing using an electrically conductive diamond tip. Microscopic three-dimensional manufacturing mainly relies on etching, deposition, and lithography. Therefore, a special emphasis was placed on nanomechanical processes, mechanochemical reaction by potassium hydroxide solution etching, and mechanical and electrical approaches. Several important surface characterization techniques consisting of scanning tunneling microscopy and related techniques, such as scanning probe microscopy and AFM, were also discussed.

1. Introduction

Nanoelectronic devices and nanomachines could soon be manufactured by manipulating atoms and molecules [1]. Microfabrication is essential for the development of these nanotechnologies but remains challenging. Conventional microfabrication relies on lithography, the most common semiconductor manufacturing technology, which is usually combined with deposition and dry and wet etching processes. More recently, new nanoprocessing methods, such as nanoprinting and molecular self-organization, have emerged with the development of nanotechnology, but these methods are limited by the shape and dimensions of workpiece materials.

Mechanical processing methods that transcribe a tool locus can produce three-dimensional microshapes with high precision using the tribological properties of tool geometry and a workpiece [2]. For example, a 1 μm wide knife edge can be formed by fine abrasive grinding [3]. Using microtribological action and degrees of freedom of materials, the shape and size of processed objects can increase if shape processing is achievable at the micron and nanometer scales [4, 5]. Therefore, microfabrication applications can be significantly extended through such novel processes [2–10].

Meanwhile, processing methods combining chemical and mechanical actions have been widely used to machine high-quality surfaces with high precision [3]. Mechanochemical processing (MCP) is a machining method that utilizes mechanical energy to activate chemical reactions and structural changes [11], providing highly flat surfaces with few defects. Recently, chemical-mechanical polishing (CMP) has been applied in the fine processing of semiconductor devices. Furthermore, a complex chemical grinding approach that combines chemical potassium hydroxide (KOH) solution etching and mechanical action has been studied, thereby improving the processing properties of CMP [3].

In recent years, maskless and friction-induced processing techniques have been utilized for nanofabrication [12–21]. The elevated internal stress and plastic deformation of masks formed at high load resulted in highly damaged mask surfaces and oxidation layers [17–21]. Mechanically processed mask patterns obtained from plastically deformed

damaged layers withstood the selective wet etching processes conducted for pattern transfer called maskless patterning or friction-induced fabrication [17–23]. The mechanistic evaluation of these processes showed that plastic deformation and oxidation layers may block the reactive KOH solution layer. Therefore, the damage remained superficial [18–21]. In contrast, the direct patterning of etching mask was proposed to reduce damage [8–11].

Few studies have used MCP at the atomic scale. For example, marking has been assessed as a physical-thermal excitation machining approach to produce storage devices, requiring complex mechanochemical processes at the nanometer scale [9]. However, severe adhesion during silicon machining made high precision difficult to achieve. Therefore, the potential application of this approach in a liquid chemical environment was investigated [3, 24]. Furthermore, a rigid silicon cantilever bearing diamond particles was produced experimentally, making the processing characteristics of silicon clearer [25].

New processing methods can achieve high-precision and high-quality machining through combined mechanical-chemical nanofabrication approaches. During mechanical processing, tool shape machining is mostly applied to material removal. Nanosized convex shapes are very difficult to obtain with high precision on surfaces. A mechanochemical approach can circumvent this issue by mechanically promoting the reaction between atmospheric gas and surface adsorption layer.

Micromachining mainly utilizes three-dimensional microscopic manufacturing processes comprising etching, deposition, and lithography. Scanning probe microscopy (SPM) techniques, which include the most common atomic force microscopy (AFM) and scanning tunneling microscopy (STM) [26, 27], are useful for surface property evaluation. These techniques involve scanning surfaces with a tip that includes a piezoelectric element. SPM is a promising tool in the nanofabrication of functional nanometer-size materials and devices [28] because of its ability to produce such nanostructures at the atomic scale. Several researchers have also attempted to use SPM techniques for local surface deposition and modification [5, 28–30]. In particular, the so-called local oxidation has been proven highly promising for the fabrication of electronic devices at the nanometer scale [31–33]. In this method, under room temperature conditions, oxidizing agents contained in the surface adsorbed water drifted across the silicon oxide layer under the influence of a high electric field, which was produced by voltage applied to the SPM probe [2, 33]. This SPM-generated oxide can function as a mask for the etching step and insulating barrier.

Mechanical friction has also been exploited using AFM in contact mode in air to fabricate silicon nanostructures on a H-passivated Si(100) substrate [34]. An AFM diamond tip sliding on a silicon surface formed protuberances on the substrate under ambient conditions [35–37]. A proper mechanical action of the sliding tip on the silicon surface resulted in local mechanochemical oxidation [35, 36]. Conversely, CMP has achieved the damage-free and high-accuracy processing of silicon wafers. If diamond tip sliding results in suitable mechanochemical action on the silicon surface, local oxidation can be performed without damaging the oxide mask during the selective wet etching process used for pattern transfer [35–38].

A similar AFM nanoprocessing method has previou- sly been developed and evaluated in our research group on a Si(100) surface without bias voltage [35–40]. The mechanochemical reaction used a conductive diamond tip with superior wear resistance and produced nanoprotuberances and grooves under ambient conditions. A KOH solution selectively etched the unprocessed silicon area, leaving processed surfaces mostly intact [35–38]. An AFM investigation was conducted to evaluate the KOH etching of silicon specimens that were initially processed by diamond tip sliding at low and high scanning densities at different rates, confirming this observation [38]. These results suggested that an approach combining mechanical and electrical processes, such as an AFM technique that simultaneously used mechanical load and bias voltage, could be developed. Previous electrical nanoprocessing systems [41] indicated that this complex approach should use a conductive diamond tip. The mechanism of this complex approach was compared to those of the mechanical and electrical processes [41]. Investigations of fundamental nanostructure characteristics are expected to provide a better understanding of the morphological and electric properties of processed areas, which is crucial to process improvement. Conductive atomic force microscopy (CAFM) has been shown to directly determine the local conductivity distribution, which is independent of topography [38, 42]. However, the local structure and electric properties of these nanostructures remain poorly understood because of their complexity.

This paper reviews the most recent developments in (1) silicon nanoprocessing through mechanochemical reaction by diamond tip sliding, followed by (2) KOH solution etching using the processed area as a mask, and (3) nanofabrication through mechanical and electrical processes using a conductive diamond tip.

2. Silicon Nanoprocessing through Mechanochemical Reaction and Etching

Several mechanochemical techniques have been developed for silicon nanoprocessing using natural pyramidal AFM diamond tips of various radii [40, 43]. The diamond tips were fabricated by polishing, and their radii were estimated by tracing on a standard sample. MCP by diamond tip sliding and the resulting silicon protuberances and grooves were evaluated by AFM *in situ* under atmospheric conditions. Sharp tips produced grooves, whereas wide tips produced protuberances on the silicon surfaces. KOH etching of the mechanochemically processed surfaces revealed that protuberance-covered areas were barely etched. In other words, processed areas that displayed a plastic deformation also acted as etching masks for the KOH solution. Three-dimensional nanoprofiles, which consisted of squares ($1000 \times 1000\,\mathrm{nm}^2$), lines interspaced by 200 nm intervals, and a two-step table, were fabricated on silicon using similarly oxidized areas as etching masks. Using thick masks that

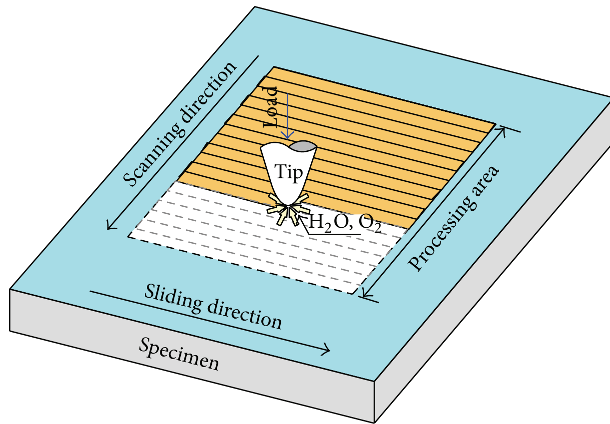

Figure 1: Mechanochemical processing of silicon by AFM tip sliding.

were mechanochemically oxidized at high load and mechanical removal of the natural oxide layer at low load, three-dimensional nanometer-sized profiles were processed by additional KOH solution etching.

To clarify the mechanism of this approach, the contact stress was analyzed using the boundary element method [40].

2.1. Processing Methods. The effects of load and diamond tip radius on the height and depth of features obtained through MCP by diamond tip sliding were studied [36]. N-type Si(100) samples were not cleaned prior to AFM processing so that their surface was covered by a natural oxide layer, which was less than 2 nm thick. First, the surfaces were mechanochemically processed under atmospheric conditions at room temperature. During this process, the specimens were driven using a piezoelectric element. Changes in processed area profiles were examined by applying a load of 10–40 μN and expanding scanning areas. The scanning procedure (256 scan lines) is shown in Figure 1 [40]. Diamond tip radii (50, 100, and 200 nm) and applied loads were changed to control the oxidation level.

Processed areas were expected to act as etching masks; therefore, the etching properties of KOH were evaluated after AFM processing. These processed wafers were etched in a 10% KOH solution at room temperature. Differences in etching rates between processed and unprocessed areas were determined by AFM measurements at low load using the processing tip.

2.2. Dependence of Silicon Nanoprocessing on Tip Radius and Load. The dependence of silicon nanoprocessing on tip radius and load was evaluated to determine the protuberance processing properties and the deformation characteristics of processed areas. Contact pressure displayed static pressure (stress). The additional stress generated during processing was measured when the tip moved and slid. Therefore, changes in processed protuberance heights and plastic deformation characteristics of processed area were investigated by measuring principal contact and shear stresses. The principal contact and shear stress of 50 and 200 nm radius diamond tips were analyzed through the boundary element method. Load effects on maximum principle and shear stresses were also studied.

Figure 2(a) shows a square silicon area (1 μm^2) processed using a tip with a 50 nm radius under an applied load of 10–40 μN, along with its section profiles (Figure 2(a) (I–III)) [40]. The AFM profile suggests that plastic deformation or cutting debris accumulated at the periphery of the processed square. The 50 nm tip produced grooves whose depth reached 20 nm and increased with increasing load on the silicon surface. AFM imaging showed that small-radius tips could remove silicon from the surface at loads as low as 10 μN.

In contrast, a 200 nm radius diamond tip produced 0–2 nm high silicon protuberances, as shown by the profiles of processed silicon square area (1 μm^2) (Figure 2(b)). The section profiles (Figure 2(b) (I–III)) also suggested that protuberance height increased with increasing applied load (50–80 μN). For example, an 80 μN load formed 1.5 nm high protuberances.

Diamond tips with radii of 100 nm simultaneously produced protuberances and grooves, as shown in Figure 2(c). Section profiles (Figure 2(c) (I–III)) revealed that protuberances appeared at loads as low as 50 μN, and grooves formed at loads as high as 70–80 μN.

Figure 3 shows the effects of tip radius and load on protuberance height and groove depth for radii of 50, 100, and 200 nm. The maximum height was obtained at a load of 40 μN using the 100 nm radius tip. In contrast, the groove depth significantly increased at a load of 40 μN and reached a maximum of 7 nm at a load of 80 μN with the 50 nm radius tip.

These AFM measurements suggest that protuberances may originate from the mechanochemical action of tip sliding on the sample. Protuberances have not been observed under vacuum and dry nitrogen conditions [44]. The mechanochemical reaction of silicon with carbon appeared to be enhanced with rising temperature under vacuum, but protuberances did not form. Protuberances have been produced using other tip materials, such as silicon nitride or silicon, but the mechanochemical reaction between silicon and diamond was negligible. Protuberances were difficult to detect when the diamond tip was used under dry conditions (less than 40% humidity), suggesting that the presence of water on the silicon surface contributes to the mechanochemical reaction.

Mechanistic models of protuberance and groove processed by diamond tip sliding were proposed using the processing characteristics. Models for height-increasing and height-decreasing processes [37] are shown in Figures 4(a) and 4(b), respectively. These protuberance processing phenomena may stem from the local atomic destruction of bonds concomitant with concentrated stress. Sliding enhances the reaction of damaged silicon with oxygen and water that are present on the surface due to the destruction of silicon–silicon bonds. This reaction forms silicon oxide (SiO_x) or silicon hydroxide ($Si(OH)_x$), increasing the height of the processed parts. The mechanochemically processed layer thickness is greater than the protuberance height.

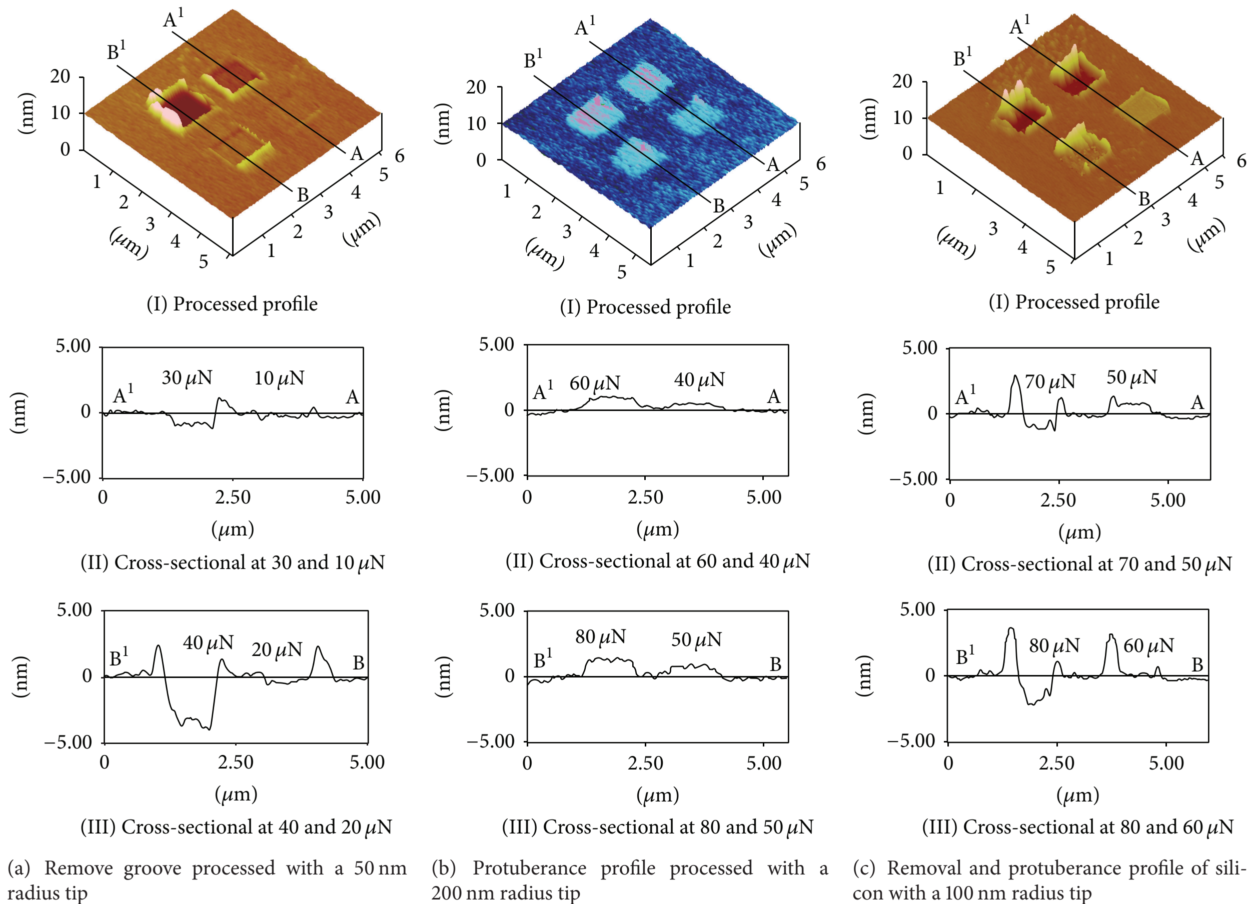

Figure 2: AFM profiles of silicon square areas processed by diamond tip sliding for different tip radii. (a) 50, (b) 200, and (c) 100 nm.

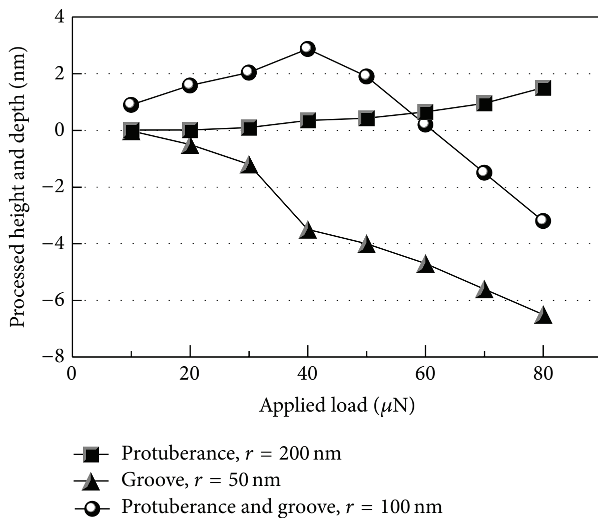

Figure 3: Tip radius and load effects on protuberance height and groove depth.

When the radius equaled 50 or 100 nm with a higher applied load, the maximum surface shearing stress exceeded the strength of silicon, leading to plastic deformation followed by the sliding-induced silicon removal from the sides and front. However, during plastic deformation, oxygen and water also reacted mechanochemically with silicon through a reaction similar to that occurring during the height-increasing process (Figure 2(b)). The nanoindentation hardness of processed protuberances and grooves was approximately 10% higher than that of unprocessed parts. The reaction of silicon with surface water and oxygen produces $Si(OH)_x$ or SiO_x, which exhibits the same hardness as silicon and is harder than $Si(OH)_x$. Therefore, instead of soft silicon hydroxide, a silicon oxide layer is speculated to form on processed protuberance and groove surfaces.

To clarify the mechanism of mechanochemical protuberance and groove processing, the surface contact stress was evaluated using the boundary element method [40]. Contact model and material parameters are presented in Figure 5. Figures 6 and 7 show the contact principal stress and shearing stress, respectively, of 50 and 200 nm radius diamond tips analyzed by the boundary element method [40]. Maximum principal stress and shearing stress dependences on load are shown in Figure 8. Hard and brittle materials such as silicon are easily fractured under tensile stress. In maximum tensile stress areas, silicon bonds appear to break under

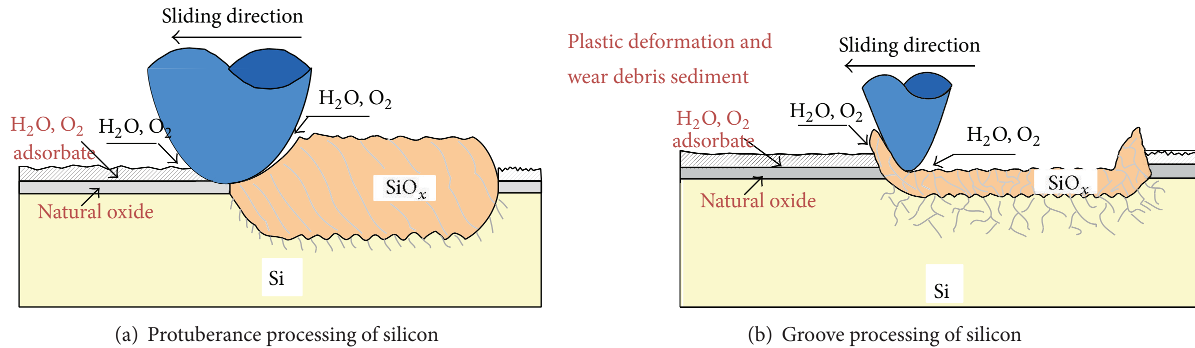

(a) Protuberance processing of silicon

(b) Groove processing of silicon

FIGURE 4: Mechanistic models for (a) protuberance and (b) groove processing by diamond tip sliding.

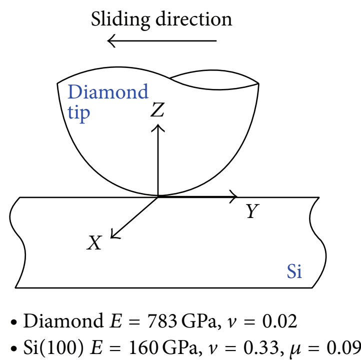

FIGURE 5: Contact stress analysis using the boundary element method.

tensile stress caused by the friction of the diamond tip. Therefore, the reaction of silicon may occur at the rear edge of the sliding contact area where the elongation stress is the highest. This protuberance processing phenomenon accompanies mechanochemical reaction during which tensile stress increases. Its mechanism may involve adsorbates, such as surface water and oxygen, which mechanochemically react with silicon [40].

Shearing stress was evaluated to estimate the plastic deformation of silicon. The effect of the evaluated contact stress on protuberance heights and groove depths is shown in Figure 9 [40]. Protuberance heights increased until the tensile stress reached 4.5 GPa and decreased. At this peak height, the maximum shear stress attained more than 8 GPa. This suggests that MCP using a 100 nm radius diamond tip is load dependent when the shear stress exceeds the strength of silicon, including a plastic deformation of several nanometers. At lower loads, the 100 nm radius tip provided protuberances through silicon oxidation. However, the maximum shear stress increased beyond the yield criterion with increasing load, resulting in silicon removal from the side and front surfaces and a subsequent decrease in protuberances height. Conversely, the tensile stress at the rear edge increased with increasing load during this removal process, indicating that water and oxygen reacted with silicon, and a mechanochemical reaction similar to the protuberance height-increasing process occurred. The silicon oxide layer is also assumed to form on processed groove surfaces, as shown in Figure 4(b).

2.3. Additional KOH Solution Etching of Processed Areas

2.3.1. Load Dependence of KOH Solution Etching on Mechanochemically Processed Areas. The KOH solution etching of a mechanically processed area is shown in Figure 10 [40]. Thick oxidized layers were mechanochemically formed on the processed areas, and these locally oxidized parts were expected to work as etching masks for KOH solution [37, 40, 43]. For short KOH etching times, the area processed at a high scanning density and the unprocessed area covered with a natural oxidative layer acted as masks and were not etched, enabling various types of nanofabrication processes via mechanochemical action. Nanoscale local oxidation based on mechanochemical action may find application in future nanodevice processes and nanolithography technology.

The effects of KOH etching on protuberance and groove processing on silicon were investigated at room temperature. Silicon protuberance and groove processing were conducted in air using a 140 nm radius diamond tip on a 1 μm^2 square area at loads ranging from 10 to 90 μN [43]. As shown in Figure 11(a), protuberance heights remained below 1 nm for 10–30 μN loads, but they increased to 1-2 nm for loads of 40, 50, and 60 μN, indicating that protuberance heights increased with increasing applied load. However, loads of 70, 80, and 90 μN generated grooves on the processed areas as well as plastic deformation. The maximum depth of the grooves was 4.5 nm. These results are in between those obtained using the 100 and 200 nm radius tips.

Silicon samples processed at loads ranging from 0 to 90 μN were etched using KOH solution for 10 min. Figure 11(b) shows that unprocessed areas were etched, whereas all processed areas remained almost intact. Processed features protruded over the surface because of KOH etching, reaching a maximum height of 8 nm. Areas processed by tip sliding clearly showed an erosion resistance to KOH solution. For high loads of 70, 80, and 90 μN, the shape of plastically deformed areas did not change after etching in KOH solution. The etching speed of processed areas with inherent defects was accelerated under normal processing conditions [37, 38], but the processed regions could not be

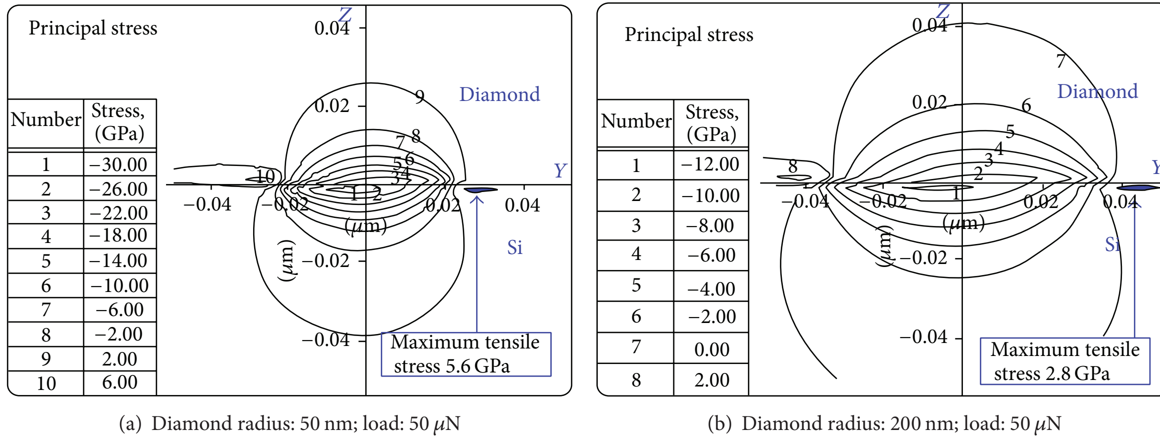

(a) Diamond radius: 50 nm; load: 50 μN (b) Diamond radius: 200 nm; load: 50 μN

FIGURE 6: Principal stress of the silicon-diamond contact area at 50 μN load for tip radii of (a) 50 and (b) 200 nm.

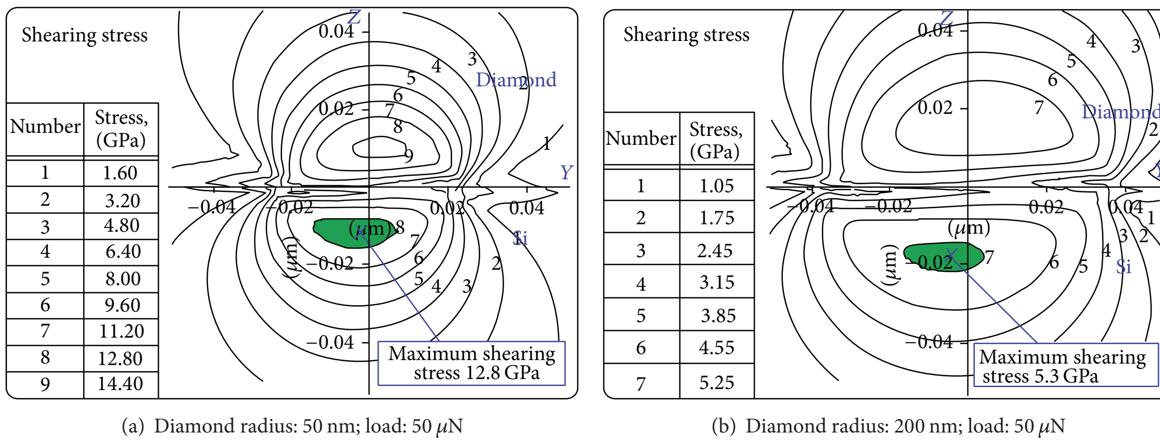

(a) Diamond radius: 50 nm; load: 50 μN (b) Diamond radius: 200 nm; load: 50 μN

FIGURE 7: Shear stress of the silicon-diamond contact area at 50 μN load for tip radii of (a) 50 and (b) 200 nm.

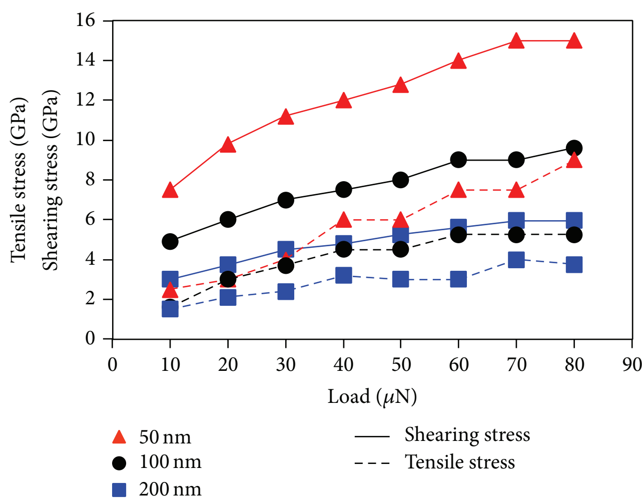

FIGURE 8: Load effects on maximum principle and shear stresses.

etched, even with plastic deformation. This may result from the formation of a dense oxide layer by tip sliding.

Figure 12(a) shows plastically deformed protuberances produced using a 100 nm radius diamond tip. The KOH solution selectively etched the unprocessed Si area, leaving protuberances and grooves processed by tip sliding unchanged. The depth of grooves processed at 80 μN was approximately 5 nm. Protuberances processed at 40 μN reached heights of nearly 1 nm. Figure 12(b) shows the surface profile after KOH solution etching for 30 min, revealing that processed protuberance and groove areas were barely etched. Height differences between processed and unprocessed areas amounted to approximately 50 nm after KOH solution etching. These results suggest that protuberances and grooves formed by diamond tip sliding consist of silicon oxide (Figure 4), which is chemically resistant to KOH. The protuberances exhibited similar upper surface profiles before and after KOH etching. Plastically deformed areas shown at the start and end of tip sliding process remained intact after KOH solution etching, suggesting the formation of silicon oxide on these areas.

Figure 13 shows the profiles of three square areas (a) processed by AFM and (b) etched using KOH [40]. Mean protuberance heights of 2.3, 2.1, and 1.2 nm were obtained by diamond tip sliding for loads of 50, 40, and 30 μN,

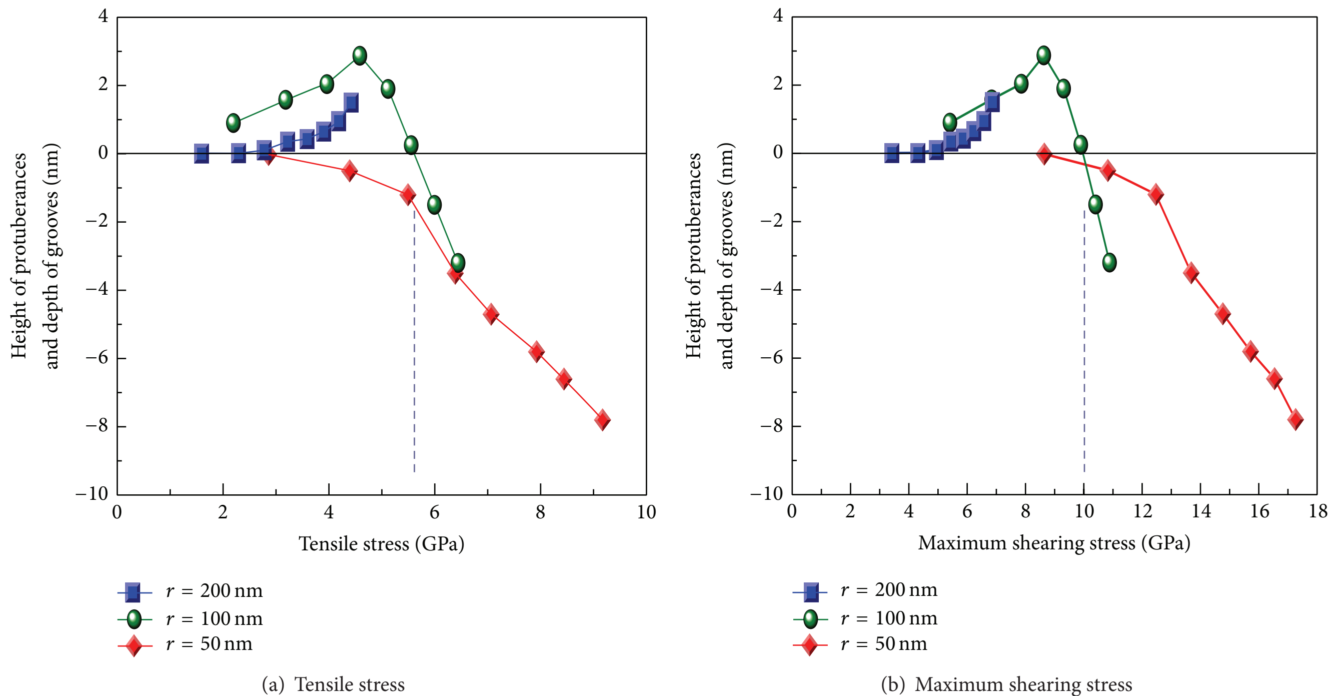

Figure 9: Contact stress effects on protuberance heights and groove depths. (a) Tensile stress effect and (b) maximum shear stress effect.

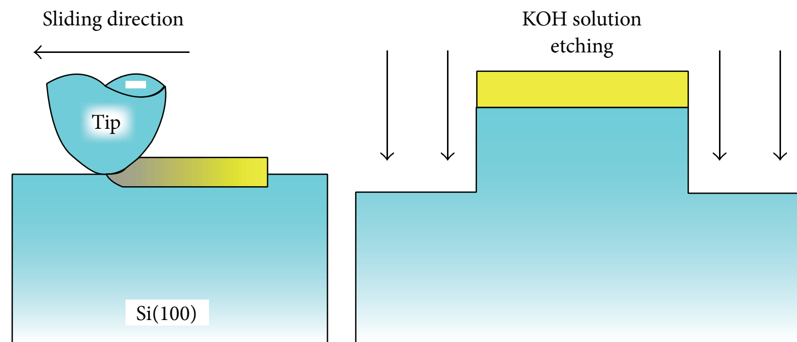

Figure 10: Profile etching model of silicon using a mechanochemically oxidized mask.

respectively. At higher loads, the plastically deformed debris accumulated at the end of the sliding. Three squares with mean heights of 82, 80, and 78 nm were clearly observed after etching. The lower profile of the KOH etched surface (Figure 13(b)) matched that of the upper profile for AFM tip processed surface (Figure 13(a)), indicating that the three processed squares were barely etched.

Figure 14 shows the profiles of lines and spaces produced by tip sliding at 50 μN before and after KOH solution etching [40]. The 2 μm long lines were interspaced by intervals of (a) 500, (b) 400, (c) 300, and (d) 200 nm. The sliding scar of the processed lines was barely visible by AFM. After KOH solution etching, four lines were clearly observed and displayed rounded ends because of side etching. Line heights ranged from 40 to 42 nm, while line spacing narrowed to 200 nm. Even without changing the profiles, tip sliding forms a silicon oxide layer that protects the processed surface from KOH etching.

2.3.2. Load and Scanning Density Effects on the KOH Solution Etching Rates of Mechanochemically Processed Areas. Figure 15(a) shows the process used to control etching rates by changing the tip loads [37, 38, 40]. A uniform natural oxide layer was formed on the silicon surface before processing (Figure 15(a)). The mechanochemically processed area exhibited a thick oxidized layer at a high load and high-density scanning (Figure 15(b)), while a low load and low-density scanning mechanically removed the natural oxide layer (Figure 15(c)).

Figure 16 shows a two-step table obtained from mechanochemically processed areas etched using KOH solution at

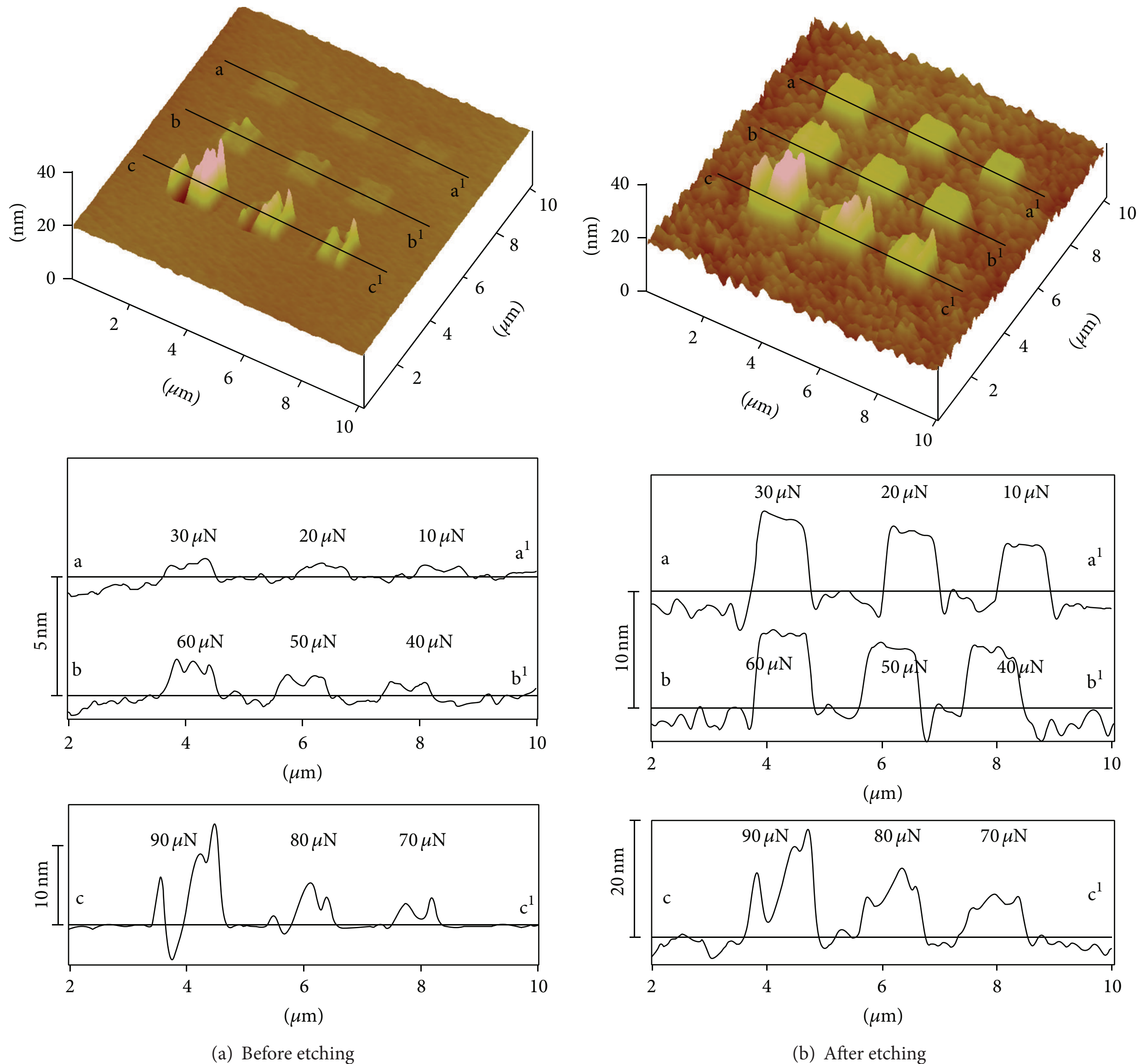

(a) Before etching

(b) After etching

FIGURE 11: Load effects on protuberance and groove processing using a 140 nm radius tip (a) before and (b) after KOH solution etching.

different rates [40]. To change the degree of oxidation of the processed area, the atomic force between the Si(100) surface and tip was changed. First, a high square protuberance of 0.6 nm ($2 \times 2\,\mu m^2$) was processed at $25\,\mu$N (Figure 16(a)). Next, a second area ($5 \times 5\,\mu m^2$) was processed at a low load and low-density scanning. Profiles obtained after additional KOH solution etching revealed that a low load and low-density scanning resulted in a thin, $5 \times 5\,\mu m^2$ oxidized area, and a high load and high-density scanning resulted in a dense, $2 \times 2\,\mu m^2$ oxidized area on the same surface ($10 \times 10\,\mu m^2$, Figure 16(b)). Load and scanning density changes during MCP can influence reaction rates. The height difference between the processed areas amounted to approximately 18 nm and total height was 33 nm, evidence for the potential fabrication of a nanometer-size two-step table.

The profile of a processed sample was obtained, as shown in Figure 17. First, a $1 \times 1\,\mu m^2$ area was mechanically oxidized by diamond tip sliding at $40\,\mu$N and was assumed to undergo partial plastic deformation. Another $1 \times 1\,\mu m^2$ area processed at $10\,\mu$N displayed a 1.5 nm high protuberance. A $6 \times 6\,\mu m^2$ area was processed by tip sliding at $1.5\,\mu$N to remove the natural oxide layer, and the sample was etched using KOH for 25 min. Figure 17 shows the resulting three-dimensional profile of the processed areas. The profile suggests that tip sliding at $1.5\,\mu$N and over a wide area removed the natural oxide layer, promoting a deep etching of 119 nm. In contrast, the surfaces of areas processed at 10 and $40\,\mu$N exhibited little differences from the unprocessed basal plane covered with a natural oxide layer. The natural oxide layer worked as an etching mask for the unprocessed surface for 25 min

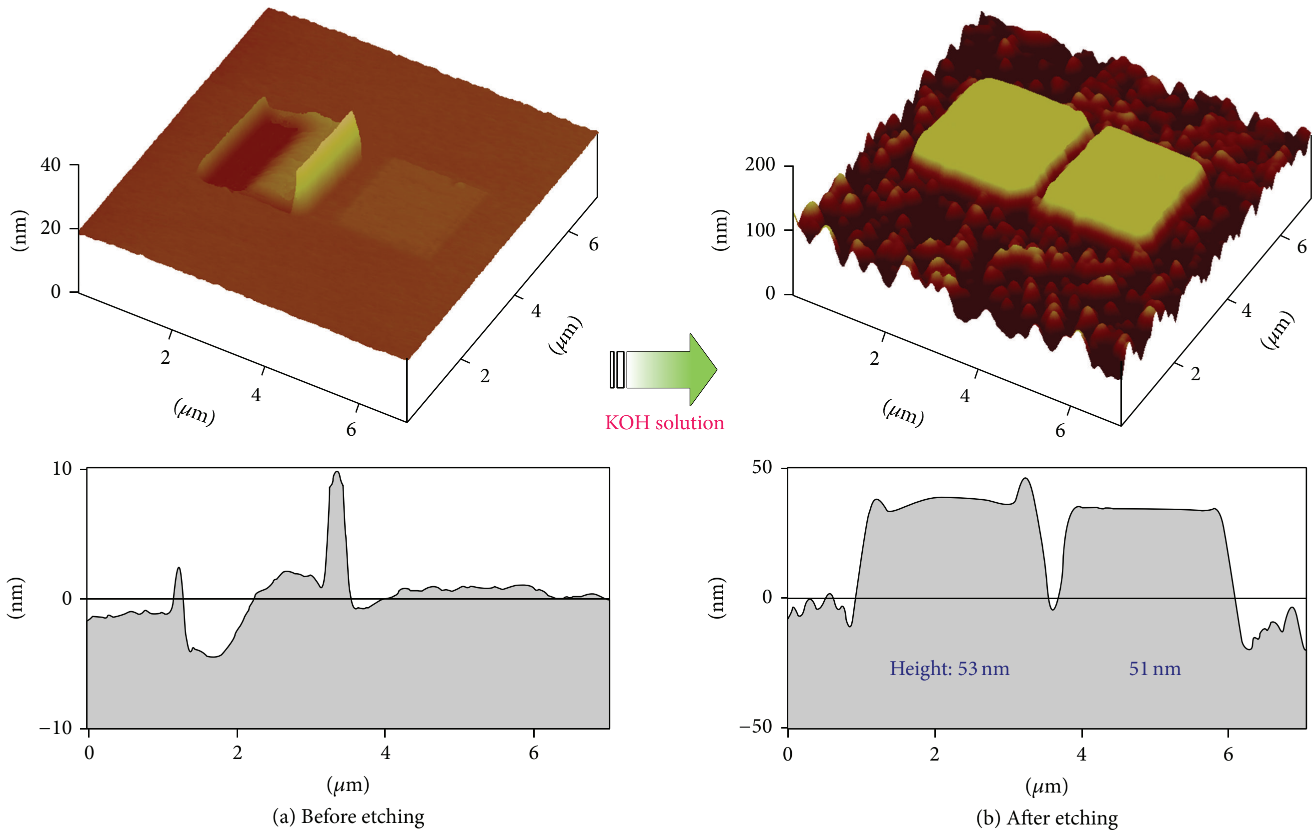

Figure 12: AFM profiles of groove and protuberance processing areas (a) before and (b) after KOH solution etching.

but, thereafter, was removed by low load and wide-range processing at 1.5 μN, increasing the etching rate.

To demonstrate this mechanism, nine squares ($1 \times 1\,\mu\text{m}^2$) were mechanically oxidized by tip sliding at 15 μN, and the processed area was expanded to a $10 \times 10\,\mu\text{m}^2$ square to remove the natural oxide layer at 1 μN. Subsequent KOH solution etching was performed for 30 min. As shown in Figure 18, the nine square areas and the unprocessed natural oxide layer were negligibly etched, indicating that they acted as etching masks.

3. Nanofabrication through Mechanical and Electrical Processes Using an Electrically Conductive Diamond Tip

Several mechanical and electrical methods, including complex combinations of both approaches, have been developed for silicon nanoprocessing using an electrically conductive diamond tip [41]. In these approaches, nanostructures were formed on naturally oxidized silicon wafers through mechanochemical and/or electrochemical reactions. Mechanochemical and electrochemical reactions were conducted by applying a load and/or electrical voltage using an electrically conductive diamond tip with a radius of approximately 45 nm. Surface morphology and electrical properties of processed areas were examined by AFM, which provides topographic and current images, as well as current-voltage (I-V) curves [41]. These investigations showed that nanostructure height and morphology depended on applied load and voltage. The electric properties of the processed regions were identified using Schottky I-V curves, which showed their dependence on the extent of local mechanochemical and electrochemical reaction generated by tip sliding during processing. In particular, complex approaches that combined mechanical and electrical processes enhanced the local oxidation at high load and voltage.

3.1. Experimental Method. Experiments were conducted using AFM apparatus with a cantilever equipped with a conductive diamond tip. Process evaluation consisted of two steps. First, sample surfaces were scanned using the tip at a relatively high contact load over a $500 \times 500\,\text{nm}^2$ area under the conditions shown in Table 1. Second, surface topography and electrical current were examined using the same tip at a low contact load of 1 nN over an enlarged scanning area ($5 \times 5\,\mu\text{m}^2$). Current images and I-V curves were generated while scanning by applying a bias voltage (0.5 V) between the sample and the conductive tip and measuring of the electrical current flowing through the tip. The reaction occurred on the ultrasmall part of the contact area, and processing time is the same for either mechanical or electrical process. The oxidation reaction was assumed to occur during processing and last as long as the processing time. The tests were

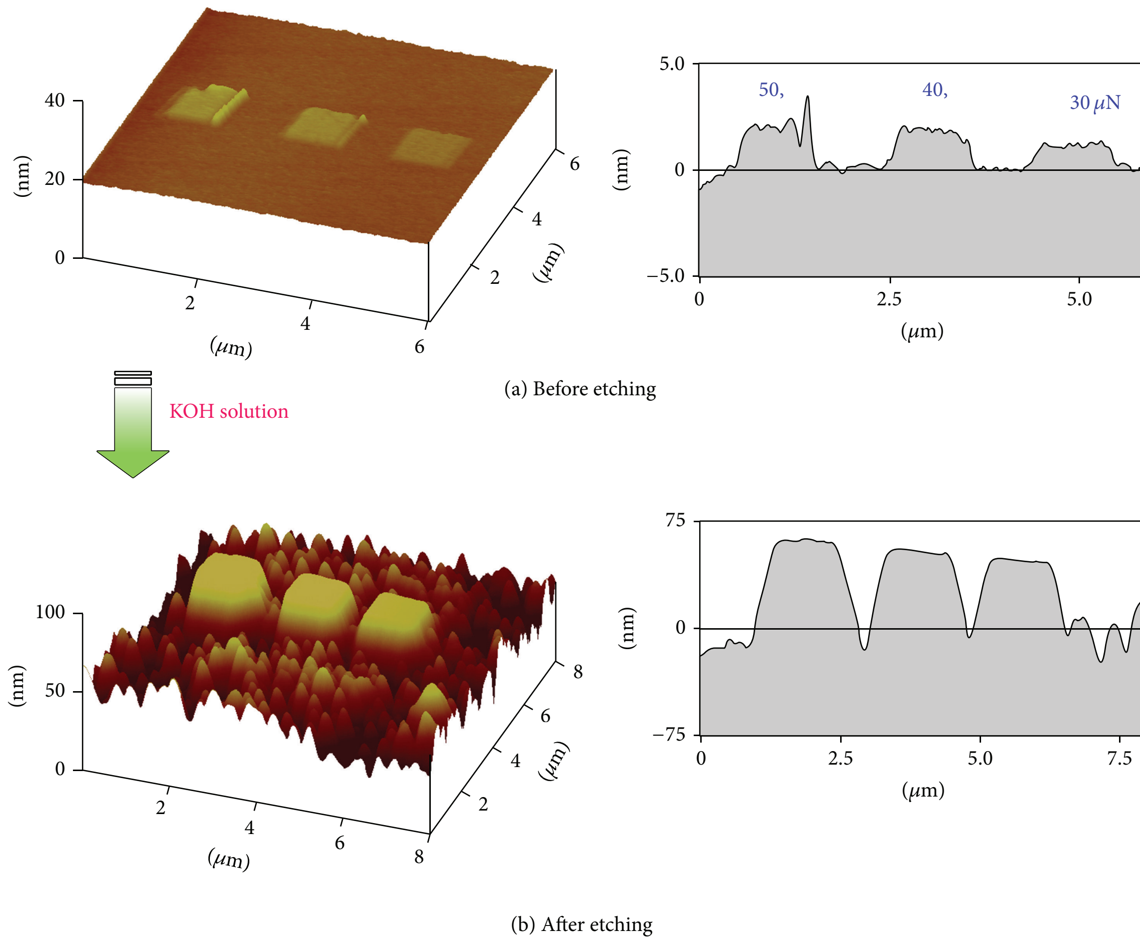

Figure 13: AFM profiles of three square areas processed at different loads (a) before and (b) after KOH solution etching.

performed three more times. Measured values were different but exhibited the same trend.

CAFM enables topography and current distribution measurements in the contact mode [41]. Furthermore, *I-V* curves of processed and unprocessed regions were obtained using an applied bias voltage because a comparison between current image and topography revealed no clear relationship between local conductivity and morphology. The probe used here consisted of a *B*-doped chemical vapor deposition diamond-coated silicon tip with a radius of approximately 45 nm and an average electrical resistance of approximately 0.0031 Ωcm at 22°C. Under ambient conditions (room temperature of approximately 22°C), the specimens were coated with an approximately 2 nm thick natural oxide layer. The cantilever ($231 \times 36\,\mu m^2$) displayed a spring constant of approximately 48 N/m and a resonance frequency of 185 kHz [41].

As shown in Figure 19, three areas (indicated by line A-A[1]) were mechanically processed by tip sliding at loads of 40, 80, and 120 nN. As indicated by line B-B[1], three areas were electrically processed by tip sliding at a load of 2 nN using bias voltages of 1, 2, and 3 V. During electrical processing, the applied force load is assumed to be 0 nN, which corresponds to a nominal zero force scan because true zero force is actually difficult to achieve. As shown by line C-C[1], mechanical and electrical processes were combined using tip sliding at nonzero loads and bias voltages. Three areas were processed through this complex electromechanical approach at loads of 40, 80, and 120 nN and voltages of 1, 2, and 3 V, respectively. Sliding tracks appear as dashed lines in Figure 19.

Table 1: Processing conditions.

Process	Load (nN)	Voltage (V)
Mechanical processing	40, 80, 120	⋯
Electrical processing	⋯	1, 2, 3
	40	1
Mechanical + electrical processing	80	2
	120	3

3.2. Surface Properties of Electrical, Mechanical, and Electromechanical Processes. Figure 20 shows the topographic images of mechanically, electrically, and electromechanically processed samples (Table 1). Along a-a[1], samples were mechanically processed by tip sliding at loads of 40, 80, and

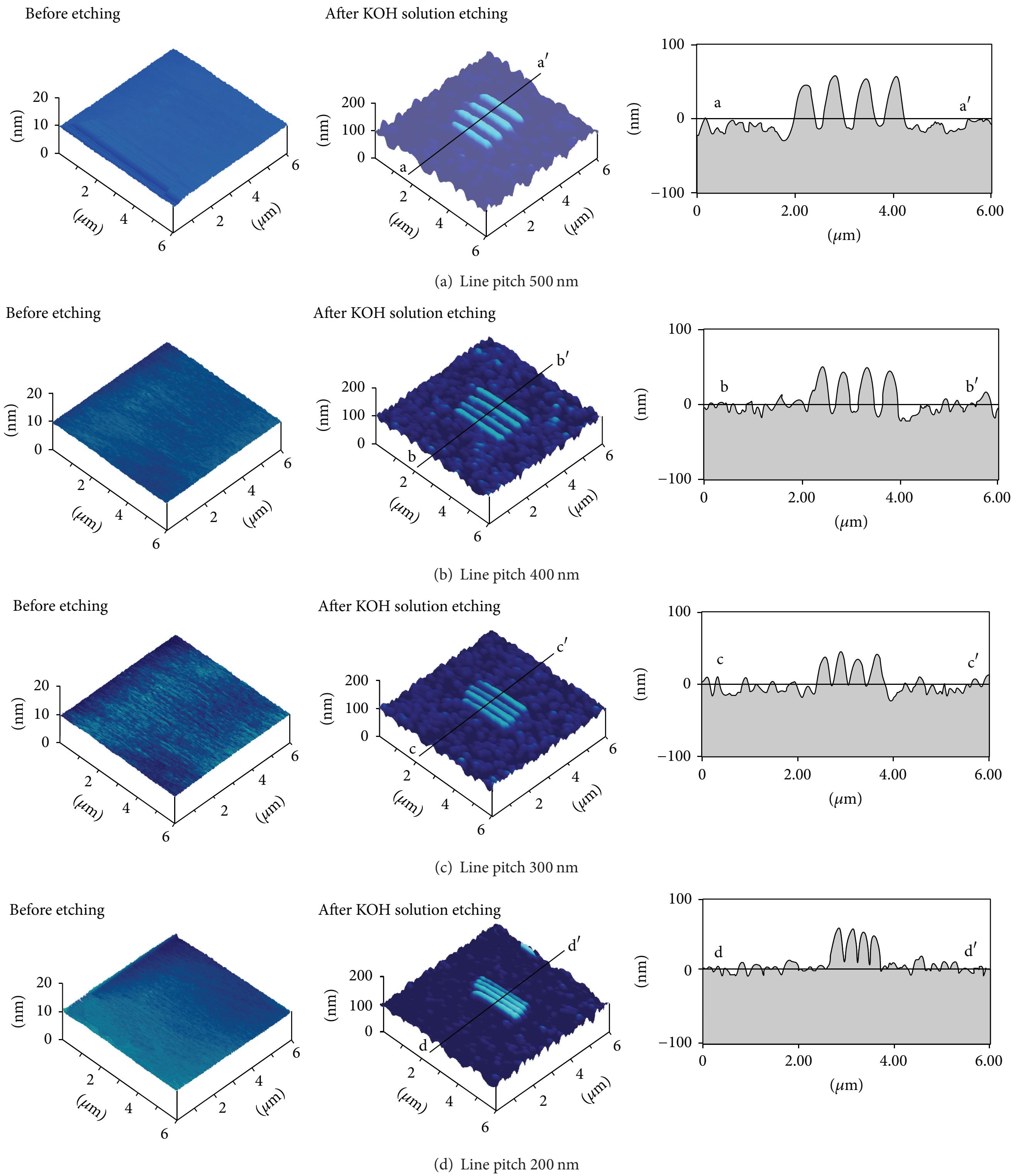

Figure 14: AFM profiles of evenly interspaced lines mechanochemically processed by tip sliding on silicon before and after etching with 10% KOH solution.

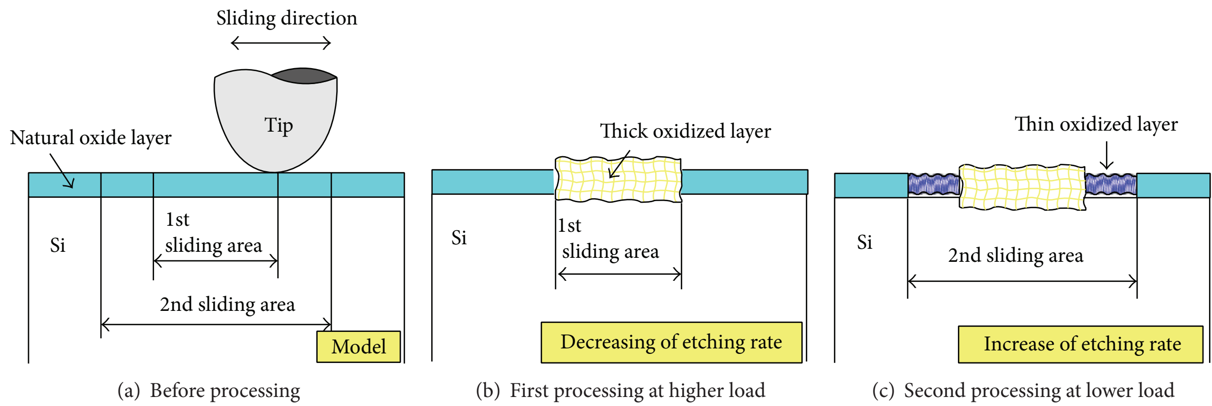

FIGURE 15: Model of a nanofabrication process using mechanochemically and naturally oxidized areas as etching masks. (a) Before processing, (b) during the first processing step at high load, and (c) during the second processing step at low load.

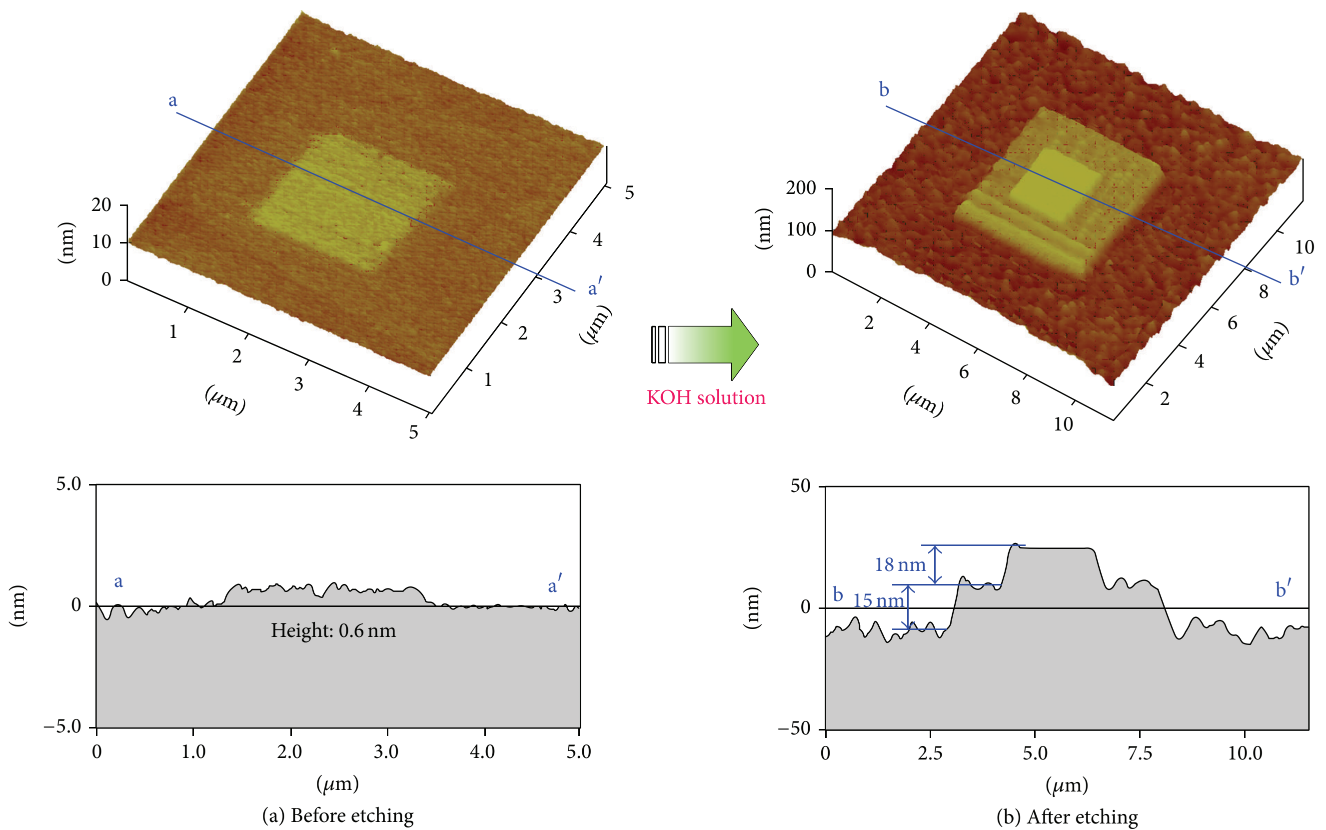

FIGURE 16: AFM profiles of a two-step table fabricated using differences in etching rates between processed areas (a) before and (b) after KOH solution etching.

120 nN, producing protuberances with heights of approximately 0.40, 0.26, and 0.20 nm, respectively. These protuberances were generated by tribochemical reaction [35, 36, 40]. In this process, protuberance heights depend on the local oxidation and plastic deformation of the specimen caused by tip sliding. Protuberance heights increased because of the tribochemical reaction. However, compression from the loading force limits protuberance growth, explaining a decrease in height with increasing load. Along b-b[1], samples were electrically processed by tip sliding using bias voltages of 1, 2, and 3 V. The applied voltage triggered an electrochemical reaction that resulted in the local oxidation of silicon. Protuberance heights of approximately 0.44, 0.50, and 0.71 nm were obtained for voltages of 1, 2, and 3 V, respectively. Protuberance heights increased with increasing voltage. The net force is assumed to strongly depend on the voltage [45, 46] so that the processing force at a load of 0 nN is substantially greater at 3 V than at 1 V. Conversely, electrical processing

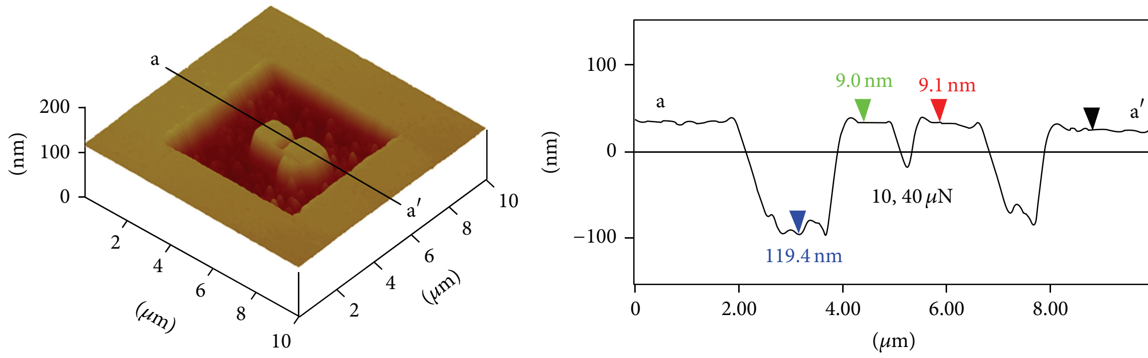

Figure 17: AFM profile obtained using mechanochemically and naturally oxidized layers as etching masks for the KOH solution.

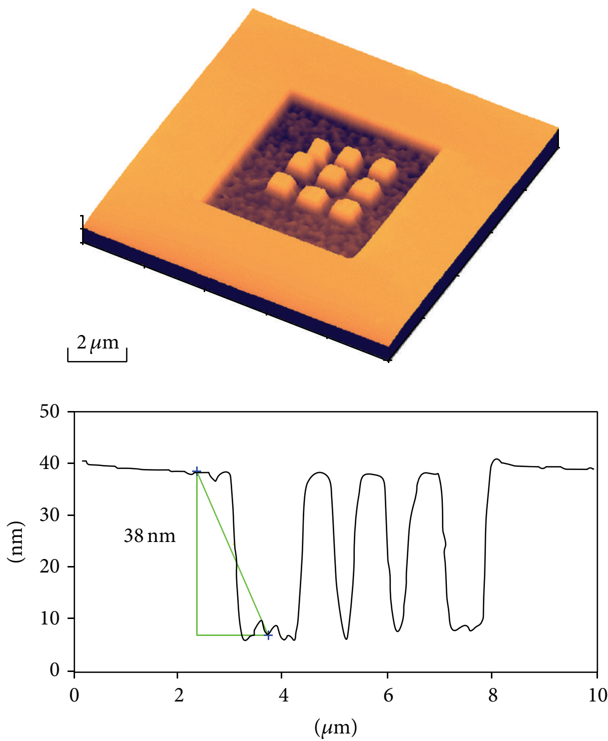

Figure 18: AFM profiles obtained using mechanochemically and naturally oxidized layers as etching masks for the KOH solution at 15 μN.

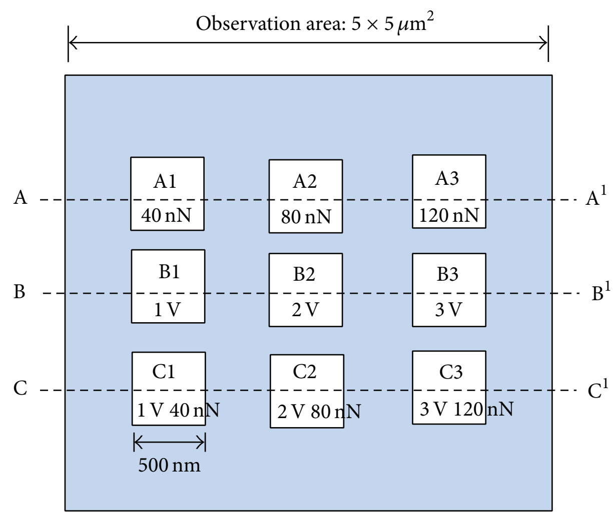

Figure 19: Scheme showing silicon square areas processed through (A-A^1) mechanical, (B-B^1) electrical, and (C-C^1) electromechanical methods at different loads and voltages.

produced taller protuberances than mechanical processing. Therefore, local oxidation may be accelerated by the voltage-induced electrochemical reaction, increasing the volume of silicon oxide formed [41].

Along c-c^1, samples were electromechanically processed by tip sliding using applied loads and voltages of 40 nN, 1 V; 80 nN, 2 V; and 120 nN, 3 V. The respective heights of the three protuberances were 0.44, 0.56, and 0.64 nm. The protuberance formed electromechanically at a 120 nN load and at 3 V was lower in height than the protuberance formed electrically at 3 V, indicating that compressive stress resulting from the high load reduced the protuberance height. This result is consistent with the reduced protuberance height being suppressed with increasing load in mechanical processing. These results also suggest that mechanical and electrical processing can effectively control the formation and growth of nanostructures through mechanochemical and electrochemical reactions. Sectional profiles showed that the electrically processed protuberances were thicker than the mechanically and electromechanically processed protuberances. It is believed that electrical action is useful in conjunction with mechanical action in protuberance fabrication. The effect of combined electrical and mechanical actions on processing is emphasized and discussed in the next section.

3.3. Electrical Properties of Electrical, Mechanical, and Electromechanical Processes. Figure 21 shows the current distribution images of areas obtained by mechanical, electrical, and electromechanical processing (Figure 20) [41]. Differences in measured current between unprocessed and processed areas were determined to compare the effect of mechanical and/or electrical techniques on fabrication. In

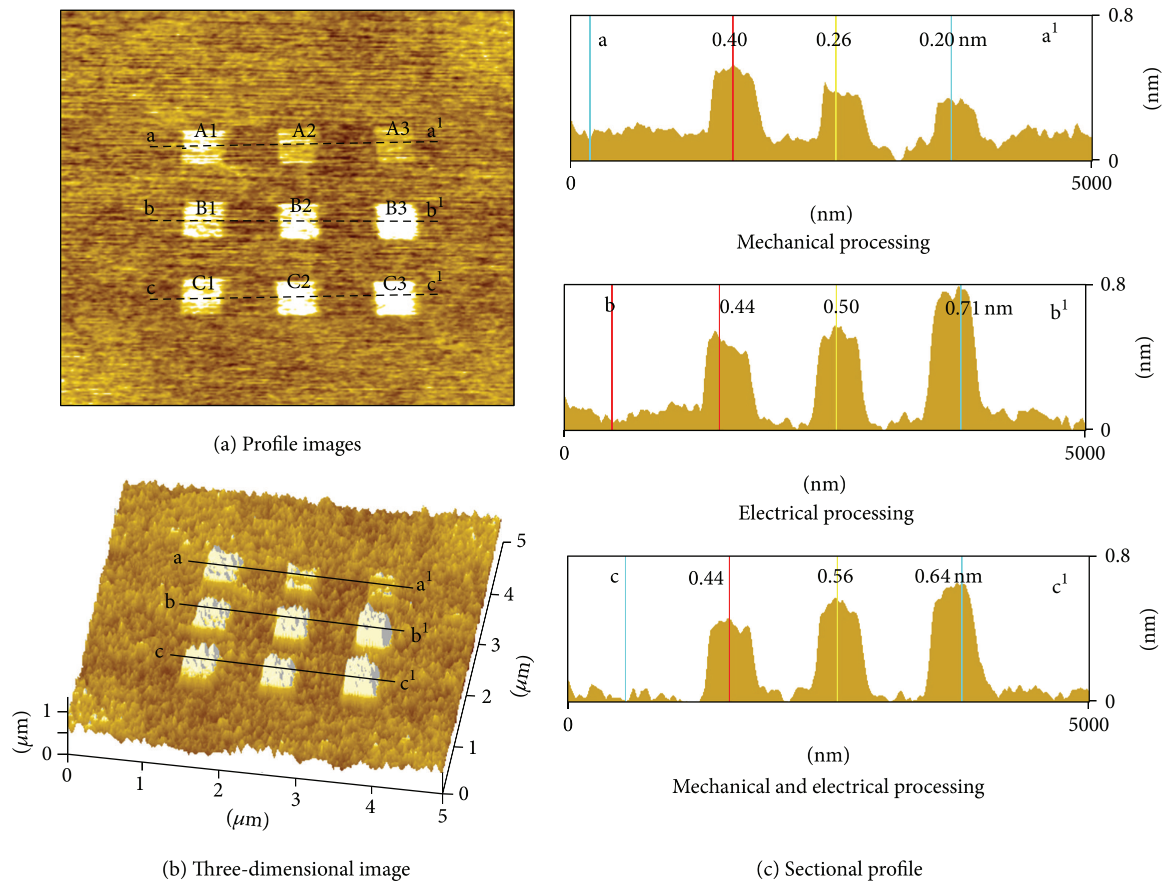

Figure 20: AFM profiles and cross-sectional images of surfaces obtained by (a) mechanical, (b) electrical, and (c) electromechanical processing.

general, processed areas displayed lower current than unprocessed areas, which stems from the formation of oxidization layers during nanoprocessing. These layers are produced by reactions between silicon and water, which included a mechanochemical reaction caused by tip sliding and an electrochemically induced anodic oxidation. A current of 0.191 nA was measured in the unprocessed area for a bias voltage of 2 V, indicating that this area was covered with an ultrathin natural oxidation layer formed under ambient conditions.

Mechanical processing resulted in current differences of 0.079, 0.077, and 0.076 nA for loads of 40, 80, and 120 nN, respectively, indicating that processed areas presented lower currents than the unprocessed areas (a-a^1, Figure 21(a)). These current differences decreased with increasing load in the processed areas, meaning that the currents increased with increasing load. This phenomenon may result from the partial removal of the oxidation layer at high load, causing its thickness to decrease.

Current differences between electrically processed and unprocessed areas amounted to 0.120, 0122, and 0.122 nA for voltages of 1, 2, and 3 V, respectively (b-b^1, Figure 21(b)). These current differences were greater than the current differences for mechanically processed samples, suggesting the formation of a thicker oxidation layer during electrical processing than during mechanical processing. This thick oxidation layer was impeded on conductivity in electrically processed areas.

Current differences between electromechanically processed and unprocessed areas equaled 0.136 nA for a 40 nN load and a voltage of 1 V, 0.137 nA for a 80 nN load and a voltage of 2 V, and 0.138 nA for a 120 nN load and a voltage of 3 V (c-c^1, Figure 21(c)), showing that currents were lower in electromechanically processed areas than in unprocessed areas. In addition, current differences increased with increasing load and voltage, concomitant with the enhanced local oxidation and plastic deformation induced by mechanical and electrochemical reactions in the processed areas. Moreover, mechanically processed areas exhibited higher average currents than electrically and electromechanically processed areas, indicating that electrical and electromechanical methods may enhance local oxidation.

Schottky *I-V* characteristics were measured to study electrical conductivity properties in unprocessed and processed areas (Figures 22–24). The detection of a breakdown voltage is expected to confirm the existence of an oxidation layer on the processed area. This layer, which hinders current flow between conductive tip and specimen, originates from the mechanically, electrically, or electromechanically induced local oxidation. Breakdown voltages obtained at different

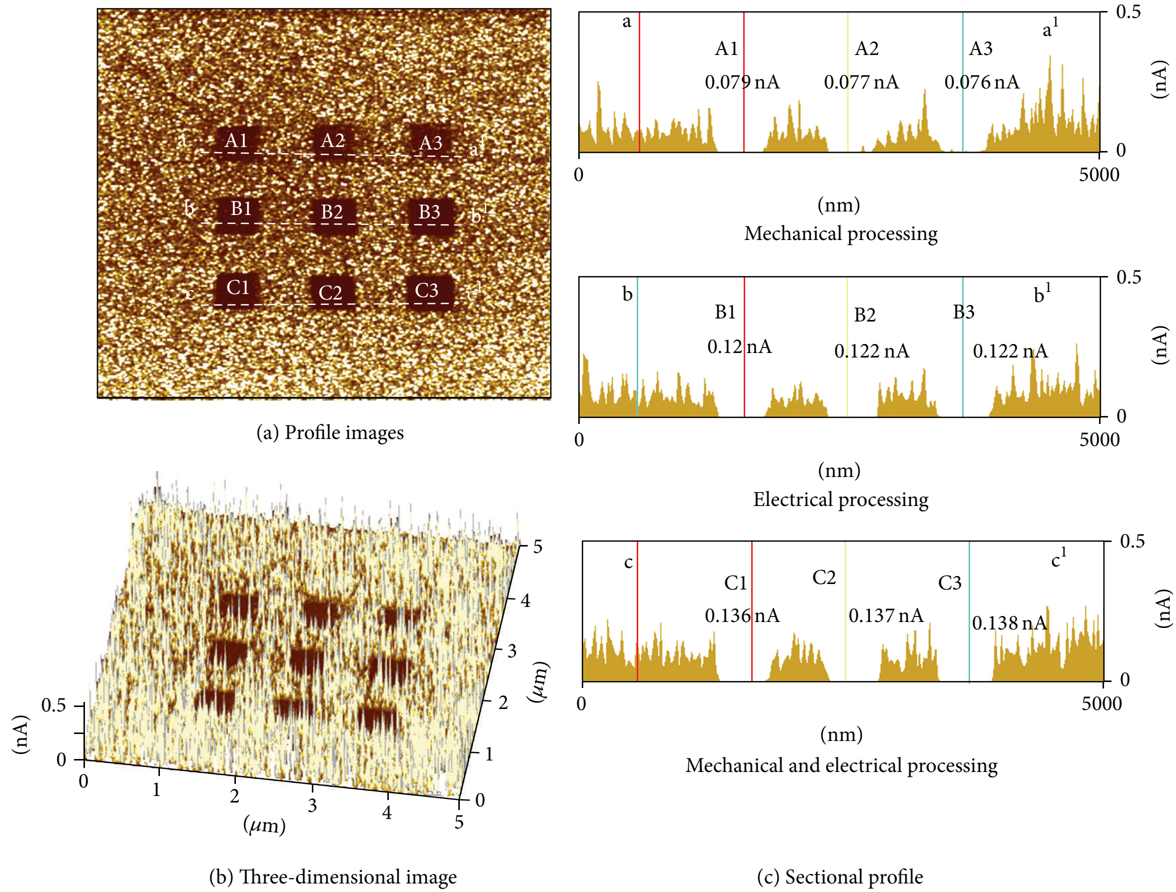

(a) Profile images

(b) Three-dimensional image

(c) Sectional profile

Figure 21: AFM current profiles and cross-sectional images of surfaces obtained by (a) mechanical, (b) electrical, and (c) electromechanical processing.

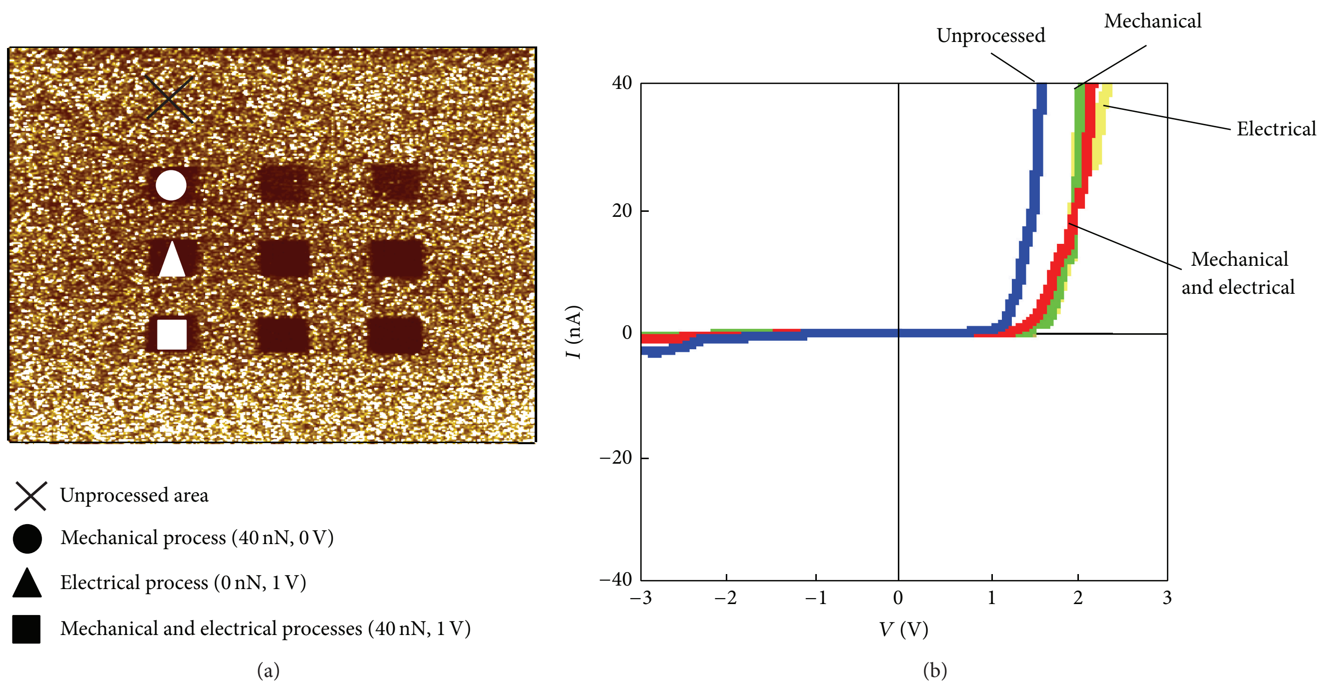

(a)

(b)

Figure 22: Surface morphology and *I-V* characteristics of areas processed at different loads and voltages of (closed circle) 40 nN, 0 V, (closed triangle) 0 nN, 1 V, and (closed square) 40 nN, 1 V.

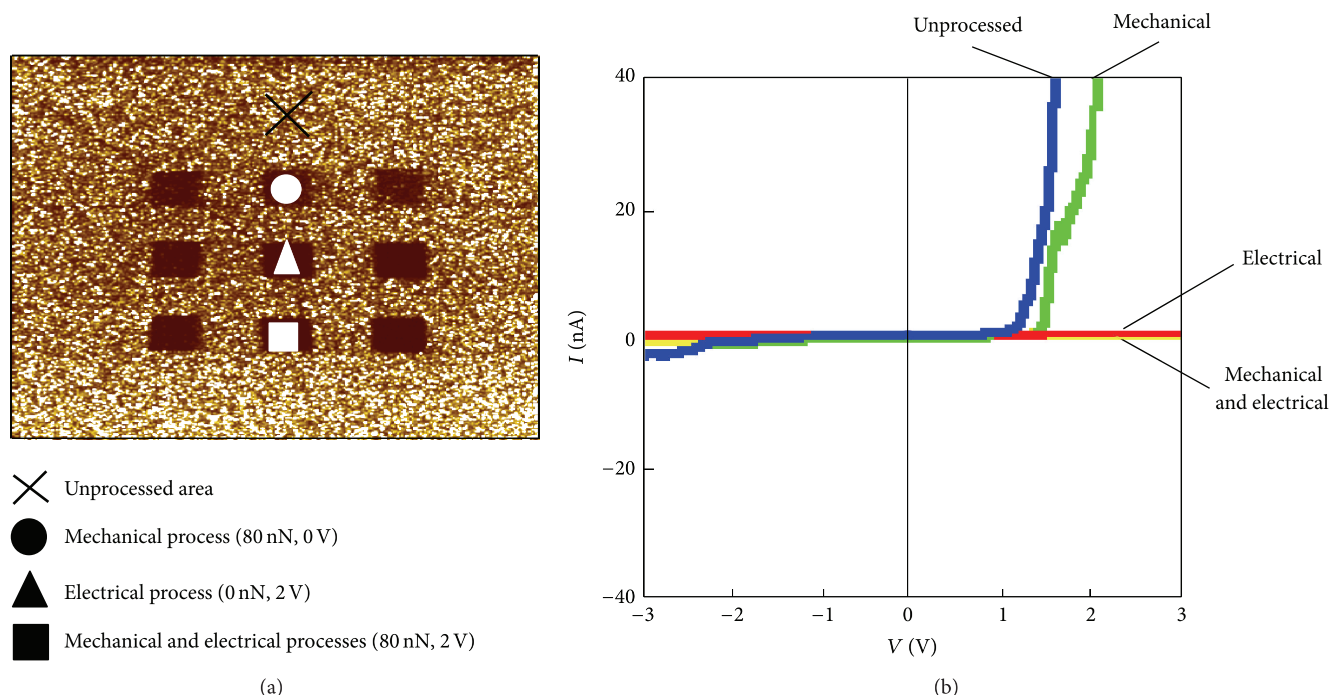

FIGURE 23: Surface morphology and *I-V* characteristics of areas processed at different loads and voltages of (closed circle) 80 nN, 0 V, (closed triangle) 0 nN, 2 V, and (closed square) 80 nN, 2 V.

processing conditions are listed in Table 2. As shown in Figure 22, breakdown voltages amounted to 1.1 V through mechanical processing at a 40 nN load (track A1), 1.1 V through electrical processing at a voltage of 1 V (track B1), and 1.08 V through electromechanical processing at a 40 nN load and a voltage of 1 V (track C1).

Figure 23 shows that the breakdown voltage increased beyond 3 V through electrical processing at a voltage of 2 V (track B2) and electromechanical processing with a 80 nN load and a voltage of 2 V (track C2). However, mechanical processing at 80 nN load (track A2) displayed breakdown voltage of approximately 1.2 V, in agreement with previous results suggesting the partial removal of the oxidation layer at high loads. In the case of electromechanical processing, the breakdown voltage increased beyond 3 V (track C2) because the oxidation was enhanced by simultaneous mechanochemical and electrochemical reactions. Figure 24 shows that the breakdown voltage increased beyond 3 V through electromechanical processing with a 120 nN load and a voltage of 3 V (track C3) due to the production of a regular and dense oxidation layer at high load and voltage. The elevated breakdown voltage of the mechanical processed area (track A3) indicates that the mechanochemical reaction enhanced the oxidation at a high load despite a reduction in protuberance height and the partial removal of the oxidation layer by tip sliding. Electrical processing also promoted the oxidation reaction with increasing bias voltage (track B3), enhancing the conductive resistance. Consequently, the breakdown voltage was higher in the electrical process than in the mechanical process. Electromechanically processed areas exhibited higher breakdown voltages than other processed areas, indicating that this complex approach can generate nanostructures with high oxidation density. Furthermore, electrical and electromechanical processing may improve nanofabrication rates because mechanochemical and electrochemical reactions enhanced oxidation rates.

4. Conclusions

This review evaluated silicon processing by diamond tip sliding under ambient conditions using AFM. First, silicon nanofabrication through AFM-based mechanical and mechanochemical processes, followed by additional KOH solution etching, was examined. Mechanochemically reacted surfaces and natural oxide layers acted as etching masks for the etching solution. Protuberances and grooves were processed on silicon surfaces in air using diamond tips with different radii. Changing the scanning density during tip sliding modulated the etching rates. Specifically, this approach was used to manufacture three-dimensional nanoprofiles, such as three squares, evenly interspaced lines, and a two-step table. Second, a CAFM-based nanofabrication technique was applied to oxidized silicon wafers. Topographic and current images, as well as *in situ I-V* characteristics of mechanically, electrically, and electromechanically processed surfaces, revealed the effects of mechanochemical and electromechanical reactions on nanofabrication. Nanoscale local oxidation based on these mechanical, mechanochemical, and electrochemical reactions may be applied to future nanodevice processes and nanolithography technology.

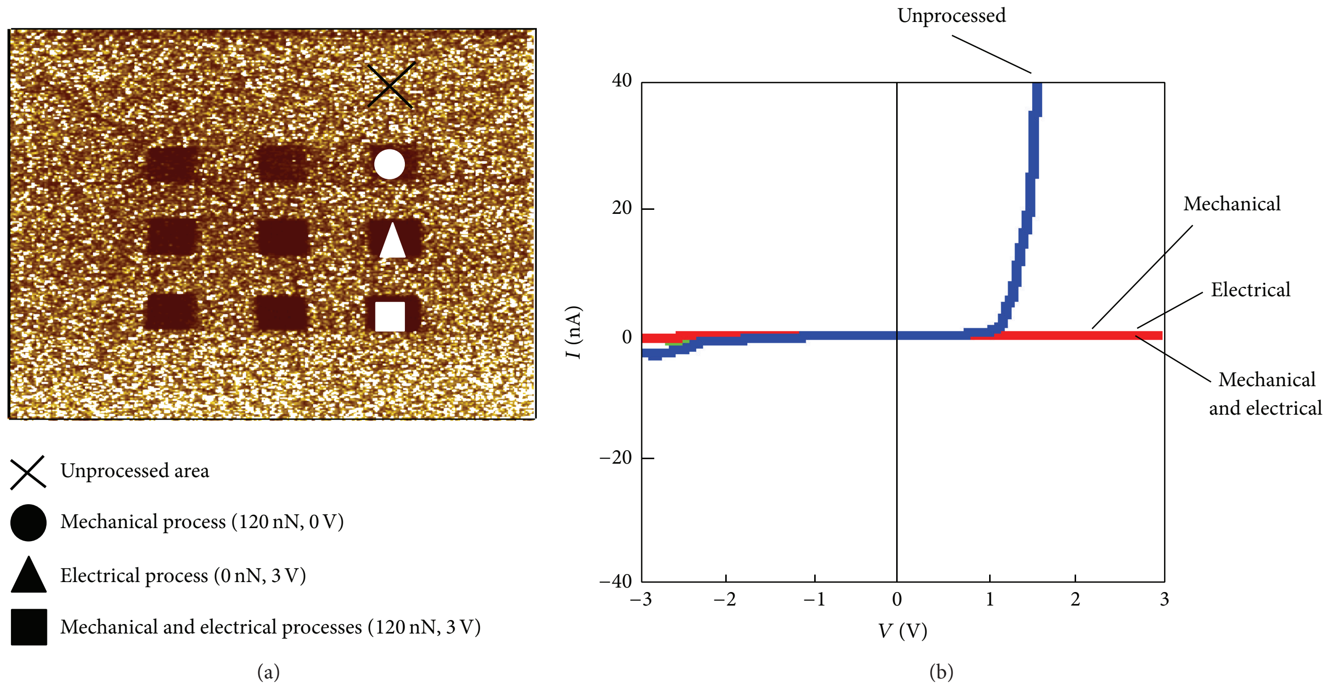

FIGURE 24: Surface morphology and *I-V* characteristic of areas processed at different loads and voltages of (closed circle) 120 nN, 0 V, (closed triangle) 0 nN, 3 V, and (closed square) 120 nN, 3 V.

TABLE 2: Breakdown voltages and processing conditions.

Processing	Tracks								
	A1	B1	C1	A2	B2	C2	A3	B3	C3
Load (nN)	40	...	40	80	...	80	120	...	120
Voltage (V)	...	1	1	...	2	2	...	3	3
Breakdown voltage (V)	1.1	1.1	1.08	1.2	3 or over	3 or over	3 or over	3 or over	3 or over

Conflict of Interests

The authors declare that there is no conflict of interests regarding the publication of this paper.

References

[1] K. E. Drexler, *Nanosystems: Molecular Machinery, Manufacturing, and Computation*, John Wiley & Sons, New York, NY, USA, 1992.

[2] S. Miyake, "Nanometer scale deposition," *Journal of the Japan Society For Precision Engineering*, vol. 59, no. 4, pp. 563–567, 1993.

[3] S. Miyake, H. Nakata, J. Watanabe, and H. Kuroda, "Face grinding of silicon wafer with resin bonded fine grained diamond wheel," *Journal of the Japan Society For Precision Engineering*, vol. 48, no. 9, pp. 1206–1212, 1982.

[4] S. Miyake, "Atomic-scale wear properties of muscovite mica evaluated by scanning probe microscopy," *Applied Physics Letters*, vol. 65, no. 8, pp. 980–982, 1994.

[5] S. Miyake, "1 nm deep mechanical processing of muscovite mica by atomic force microscopy," *Applied Physics Letters*, vol. 67, pp. 2925–2927, 1995.

[6] S. Miyake, M. Ishii, T. Otake, and N. Tsushima, "Nanometer-scale mechanical processing of muscovite mica by atomic force microscope," *Journal of the Japan Society For Precision Engineering*, vol. 63, no. 3, pp. 426–430, 1997.

[7] S. Miyake, T. Otake, and M. Asano, "Mechanical processing of standard rulers with one-nanometer depth of muscovite mica using an atomic force microscope," *Journal of the Japan Society for Precision Engineering*, vol. 65, no. 4, pp. 570–574, 1999.

[8] S. Miyake and J. Kim, "Nanoprocessing of carbon and boron nitride nanoperiod multilayer films," *Japanese Journal of Applied Physics*, vol. 42, no. 3B, pp. L322–L325, 2003.

[9] S. Miyake and K. Matsuzaki, "Mechanical nanoprocessing of layered crystal structure materials by atomic force microscopy," *Japanese Journal of Applied Physics*, vol. 41, no. 9, pp. 5706–5712, 2002.

[10] S. Miyake and M. Asano, "Nanometer-scale mechanical processing of muscovite mica and application to high-density memory," *The Institute of Electrical Engineers of Japan: Transactions on Sensors and Micromachines*, vol. 120-E, no. 1, pp. 8–14, 2000.

[11] T. Karaki, S. Miyake, and J. Watanabe, "Facilitation mechanism of polishing rate in mechano-chemical polishing of Si single crystals: a study on mechano-chemical polishing (2nd Report),"

Journal of the Japan Society of Precision Engineering, vol. 46, no. 3, pp. 331–337, 1980.

[12] L. Chen, N. Morita, and K. Ashida, "Maskless pattern formation which used alkaline etching and nano-scale cutting by using friction force microscope," *Journal of the Japan Society for Precision Engineering*, vol. 66, pp. 23–27, 2000.

[13] K. Ashia, L. Chen, and N. Morita, "New maskless micro-fabrication technique of single-crystal silicon using the combination of nanometer scale machining and wet etching," in *Proceedings of the 2nd Euspen International Conference*, pp. 78–81, Cranfield University Campus, Bedford Euspen, UK, 2001.

[14] B. Yu, X. Li, H. Dong, Y. Chen, L. Qian, and Z. Zhou, "Towards a deeper understanding of the formation of friction-induced hillocks on monocrystalline silicon," *Journal of Physics D*, vol. 45, no. 14, Article ID 145301, 2012.

[15] B. Yu, L. Qian, H. Dong, J. Yu, and Z. Zhou, "Friction-induced hillocks on monocrystalline silicon in atmosphere and in vacuum," *Wear*, vol. 268, no. 9-10, pp. 1095–1102, 2010.

[16] C. Song, X. Li, B. Yu, H. Dong, L. Qian, and Z. Zhou, "Friction-induced nanofabrication method to produce protrusive nanostructures on quartz," *Nanoscale Research Letters*, vol. 6, no. 1, pp. 310–318, 2011.

[17] B. Yu, H. Dong, L. Qian, Y. Chen, J. Yu, and Z. Zhou, "Friction-induced nanofabrication on monocrystalline silicon," *Nanotechnology*, vol. 20, no. 46, Article ID 465303, 2009.

[18] J. Guo, C. F. Song, X. Y. Li et al., "Fabrication mechanism of friction-induced selective etching on Si(100) surface," *Nanoscale Research Letters*, vol. 7, pp. 152–161, 2012.

[19] B. J. Yu and L. M. Qian, "Effect of crystal plane orientation on the friction-induced nanofabrication on monocrystalline silicon," *Nanoscale Research Letters*, vol. 8, pp. 137–144, 2013.

[20] C. F. Song, X. Y. Li, S. X. Cui, H. S. Dong, B. J. Yu, and L. M. Qian, "Maskless and low-destructive nanofabrication on quartz by friction-induced selective etching," *Nanoscale Research Letters*, vol. 8, pp. 140–147, 2013.

[21] F. Ebrahimi and L. Kalwani, "Fracture anisotropy in silicon single crystal," *Materials Science and Engineering A*, vol. 268, no. 1-2, pp. 116–126, 1999.

[22] M. H. Wang, W. Wang, and Z. S. Lu, "Anisotropy of machined surfaces involved in the ultra-precision turning of single-crystal silicon-a simulation and experimental study," *The International Journal of Advanced Manufacturing Technology*, vol. 8, pp. 473–485, 2012.

[23] P. Stempflé and J. Takadoum, "Multi-asperity nanotribological behavior of single-crystal silicon: crystallography-induced anisotropy in friction and wear," *Tribology International*, vol. 48, pp. 35–43, 2012.

[24] Y. Samitsu, "Study of atomic scale processing using an atomic force microscope," *Journal of the Japan Society for Precision Engineering*, vol. 61, no. 8, pp. 1121–1125, 1995.

[25] N. Kawasegi, N. Takano, D. Oka et al., "Nanomachining of silicon surface using atomic force microscope with diamond tip," *Journal of Manufacturing Science and Engineering, Transactions of the ASME*, vol. 128, no. 3, pp. 723–729, 2006.

[26] R. Howland and L. Benatar, *A Practical Guide to Scanning Probe Microscopy*, TM Microscopes, Sunnyvale, Calif, USA, 2000.

[27] G. Binning, H. Rohrer, C. Gerber, and E. Weibel, "Surface studies by scanning tunneling microscopy," *Physical Review Letters*, vol. 49, no. 1, pp. 57–61, 1982.

[28] C. R. K. Marrian, *Technology of Proximal Probe Lithography*, SPIE Optical Engineering, Bellingham, Wash, USA, 1993.

[29] D. M. Eigler and E. K. Schweizer, "Positioning single atoms with a scanning tunnelling microscope," *Nature*, vol. 344, no. 6266, pp. 524–526, 1990.

[30] H. J. Mamin and D. Rugar, "Thermomechanical writing with an atomic force microscope tip," *Applied Physics Letters*, vol. 61, no. 8, pp. 1003–1005, 1992.

[31] J. A. Dagata, J. Schneir, H. H. Harary, C. J. Evans, M. T. Postek, and J. Bennett, "Modification of hydrogen-passivated silicon by a scanning tunneling microscope operating in air," *Applied Physics Letters*, vol. 56, no. 20, pp. 2001–2003, 1990.

[32] L. A. Nagahara, T. Thundat, and S. M. Lindsay, "Nanolithography on semiconductor surfaces under an etching solution," *Applied Physics Letters*, vol. 57, no. 3, pp. 270–272, 1990.

[33] M. Heim, R. Eschrich, A. Hillebrand, H. F. Knapp, G. Cevc, and R. Guckenberger, "Scanning tunneling microscopy based on the conductivity of surface adsorbed water. Charge transfer between tip and sample via electrochemistry in a water meniscus or via tunneling?" *Journal of Vacuum Science & Technology B*, vol. 14, no. 20, pp. 1498–1502, 1996.

[34] H. T. Lee, J. S. Oh, S. J. Park et al., "Nanometer-scale lithography on H-passivated Si(100) with an atomic force microscope in air," *Journal of Vacuum Science & Technology A*, vol. 15, no. 3, pp. 1451–1454, 1997.

[35] S. Miyake and J. Kim, "Microprotuberance processing of silicon by diamond tip scanning," *Journal of the Japan Society for Precision Engineering*, vol. 65, no. 12, pp. 1788–1792, 1999.

[36] S. Miyake and J. Kim, "Nano protuberance and groove processing of silicon by diamond tip sliding," *The Institute of Electrical Engineers of Japan: Transactions on Sensors and Micromachines*, vol. 120-E, no. 7, pp. 350–356, 2000.

[37] S. Miyake and J. Kim, "Fabrication of silicon utilizing mechanochemical local oxidation by diamond tip sliding," *Japanese Journal of Applied Physics*, vol. 40, no. 11B, part 2, pp. L1247–L1249, 2001.

[38] S. Miyake and J. Kim, "Increase and decrease of etching rate of silicon due to diamond tip sliding by changing scanning density," *Japanese Journal of Applied Physics*, vol. 41, no. 10, pp. L1116–L1119, 2002.

[39] J. Kim and S. Miyake, "Nanometer scale protuberance and groove processing of silicon by mechano-chemical action and its application of etching mask," *Journal of the Japan Society for Precision Engineering*, vol. 68, no. 5, pp. 695–699, 2002.

[40] S. Miyake and J. Kim, "Nanoprocessing of silicon by mechanochemical reaction using atomic force microscopy and additional potassium hydroxide solution etching," *Nanotechnology*, vol. 16, no. 1, pp. 149–157, 2005.

[41] S. Miyake, H. Zheng, J. Kim, and M. Wang, "Nanofabrication by mechanical and electrical processes using electrically conductive diamond tip," *Journal of Vacuum Science and Technology B: Microelectronics and Nanometer Structures*, vol. 26, no. 5, pp. 1660–1665, 2008.

[42] L. Zhang, T. Sakai, N. Sakuma, T. Ono, and K. Nakayama, "Nanostructural conductivity and surface-potential study of low-field-emission carbon films with conductive scanning probe microscopy," *Applied Physics Letters*, vol. 75, no. 22, pp. 3527–3529, 1999.

[43] S. Miyake, M. Wang, and J. Kim, "Nano mechanical processing of silicon by atomic force microscopy," in *Key Engineering Materials*, vol. 291-292, pp. 401–406, Trans Tech Publications, 2005.

[44] Y. Ando and R. Kaneko, "Microwear process," in *Proceedings of the International Conference on Tribology*, p. 1913, JAST Press, Yokohama, Japan, 1995.

[45] E. S. Snow and P. M. Campbell, "Fabrication of Si nanostructures with an atomic force microscope," *Applied Physics Letters*, vol. 64, no. 15, pp. 1932–1934, 1994.

[46] Ph. Avouris, R. Martel, T. Hertel, and R. L. Sandström, "AFM-based fabrication of lateral single-electron tunneling structures for elevated temperature operation," *Applied Physics A Materials Science & Processing*, vol. 66, part 1-2, pp. S659–S667, 1998.

Journal of
Nanotechnology

International Journal of
Corrosion

International Journal of
Polymer Science
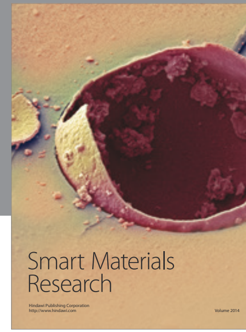
Smart Materials
Research

Journal of
Composites

BioMed
Research International

Hindawi
Submit your manuscripts at
http://www.hindawi.com
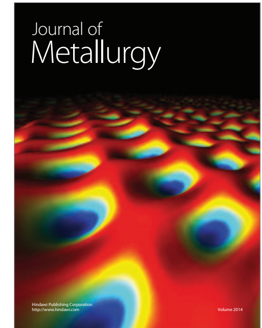
Journal of
Metallurgy

Journal of
Materials
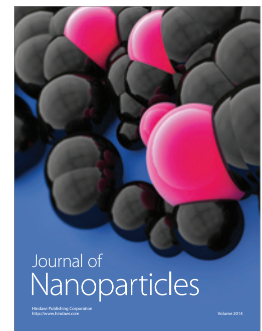
Journal of
Nanoparticles
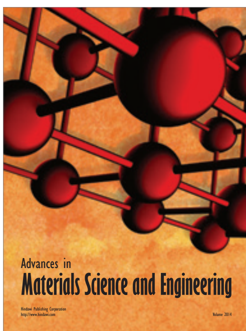
Advances in
Materials Science and Engineering
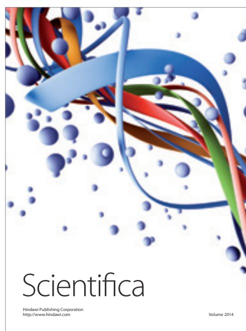
Scientifica
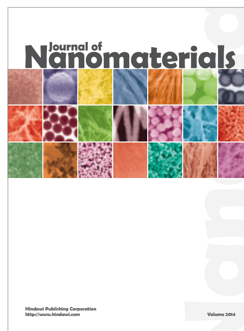
Journal of
Nanomaterials
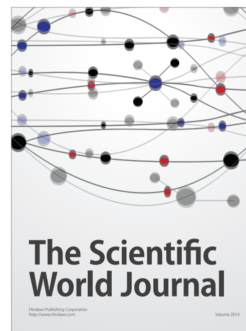
The Scientific
World Journal

International Journal of
Biomaterials

Journal of
Nanoscience

Journal of
Coatings

Journal of
Crystallography

Journal of
Ceramics

Journal of
Textiles